One-pot facile green synthesis of biocidal silver nanoparticles

Materials Research Express

PAPER

One-pot facile green synthesis of biocidal silver nanoparticles

Shabiha Nudrat Hazarika[1], **Kuldeep Gupta**[1], **Khan Naseem Ahmed Mohammed Shamin**[1], **Pushpender Bhardwaj**[1], **Ratan Boruah**[2], **Kamlesh K Yadav**[3], **Ashok Naglot**[3], **P Deb**[2], **M Mandal**[1], **Robin Doley**[1], **Vijay Veer**[4], **Indra Baruah**[4] **and Nima D Namsa**[1]

[1] Department of Molecular Biology and Biotechnology, Tezpur University (A Central University), Napaam, Tezpur, Assam 784 028, India
[2] Department of Physics, Tezpur University (A Central University), Napaam, Tezpur, Assam 784 028, India
[3] Biotechnology Division, Defence Research Laboratory, Defence R & D Organisation, Tezpur, Assam 784001, India
[4] Medical Entomology Division, Defence Research Laboratory, Defence R & D Organisation, Tezpur, Assam 784001, India

E-mail: namsa@tezu.ernet.in

Keywords: green synthesis, composites, atomic force microscopy, antimicrobial activity

Supplementary material for this article is available online

OPEN ACCESS

RECEIVED
4 February 2016

REVISED
27 May 2016

ACCEPTED FOR PUBLICATION
9 June 2016

PUBLISHED
15 July 2016

Abstract

The plant root extract mediated green synthesis method produces monodispersed spherical shape silver nanoparticles (AgNPs) with a size range of 15–30 nm as analyzed by atomic force and transmission electron microscopy. The material showed potent antibacterial and antifungal properties. Synthesized AgNPs display a characteristic surface plasmon resonance peak at 420 nm in UV–Vis spectroscopy. X-ray diffractometer analysis revealed the crystalline and face-centered cubic geometry of *in situ* prepared AgNPs. Agar well diffusion and a colony forming unit assay demonstrated the potent biocidal activity of AgNPs against *Staphylococcus aureus*, *Escherichia coli*, *Bacillus subtilis*, *Klebsiella pneumoniae*, *Pseudomonas diminuta* and *Mycobacterium smegmatis*. Intriguingly, the phytosynthesized AgNPs exhibited activity against pathogenic fungi, namely *Trichophyton rubrum*, *Aspergillus versicolor* and *Candida albicans*. Scanning electron microscopy observations indicated morphological changes in the bacterial cells incubated with silver nanoparticles. The genomic DNA isolated from the bacteria was incubated with an increasing concentration of AgNPs and the replication fidelity of 16S rDNA was observed by performing 18 and 35 cycles PCR. The replication efficiency of small (600 bp) and large (1500 bp) DNA fragments in the presence of AgNPs were compromised in a dose-dependent manner. The results suggest that the *Thalictrum foliolosum* root extract mediated synthesis of AgNPs could be used as a promising antimicrobial agent against clinical pathogens.

1. Introduction

The current research trend in the field of nanotechnology is increasing due to attractive and diversified biomedical application of metallic nanomaterials having a variable size raging from 1–100 nm. Synthesis of silver nanoparticles (AgNPs) is of much interest to the scientific community because of its wide range of applications. These AgNPs are being successfully used in cancer diagnosis and treatment as well [1, 2]. Generally, nanoparticles are prepared by a variety of chemical and physical methods which are quite expensive and potentially hazardous to the environment due to the presence of residual chemicals that are responsible for various biological risks [3]. The development of biologically-inspired experimental processes or greener approaches for the syntheses of nanoparticles is evolving into an important branch of nanotechnology. The microbial method of AgNPs synthesis requires the elaborate process of culture maintenance, purification and the adherence of bacteria or fungi on the nanoparticle surface, which raises the potential risk to human and environmental health [4–6]. Plant mediated syntheses of nanoparticles provides selective advancement over microbial methods as they are simple, one step, cost-effective, eco-friendly and relatively reproducible and often result in more stable materials [7]. A large number of plants have been reported in the literature for biosynthesis

of antimicrobial AgNPs [6]. For example, a rapid synthesis of spherical shaped antibacterial AgNPs with dimensions of 50–100 nm were observed using *Alternanthera dentate* leaf extract [8]. A stable and spherical shaped AgNP synthesized using leaf extract of *Abutilon indicum* showed high antimicrobial activities against *Salmonella typhi*, *Escherichia coli*, *Staphylococcus aureus* and *Bacillus subtilis* [9]. The leaf part of the plants have successfully been reported to perform the dual role of reduction and capping for the biosynthesis of AgNPs [6] including the tuber of *Curcuma longa* [10], the seeds of *Jatropha curcas* [11], and the fruit of *Terminalia chebula* [12]. The formation of AgNPs was observed within 30 min of the addition of the aqueous leaf extract of *Acalypha indica* and the particles exhibited antibacterial activity against water borne pathogens [13], and a similar observation of rapid biosynthesis of stable silver, gold and bi-metallic Ag/Au core–shell nanoparticles with the leaf extract of *Azadirachta indica* has been reported previously [14].

Considering the vast potentiality of plants as nanofactories, the present work aims to apply a greener technique for the synthesis of AgNPs as an alternative to conventional methods. In this study, we use the root extracts of *Thalictrum foliolosum* (TF) as a reducing and capping agent in an aqueous silver nitrate solution. TF DC is a tall perennial herb native to the temperate Himalayan region of India. In the literature, there is no report on the synthesis of nanoparticles using this plant. The first objective was to develop a simple and environmentally friendly approach for the synthesis and characterization of biocompatible AgNPs using TF. The second aim was to demonstrate the biocidal property of AgNPs against a panel of clinical pathogens such as *Escherichia coli*, *Klebsiella pneumoniae*, *Pseudomonas diminuta*, *Bacillus subtilis*, *Staphylococcus aureus*, *Mycobacterium smegmatis*, *Trichophyton rubrum, Aspergillus versicolor*, and *Candida albicans*, representing gram-negative, gram-positive and fungal strains, respectively.

2. Experimental section

2.1. Preparation of aqueous root extracts and synthesis of AgNPs

The roots of TF were freshly collected and the powdered samples were boiled in a 250 ml glass beaker for 10 min. The filtrate obtained was used for the *in situ* reduction of silver ions at physiological pH and room temperature. In a simple reaction procedure, 5 ml of TF root extract was added to 95 ml of 1×10^{-3} M aqueous $AgNO_3$ solution.

2.2. Characterization of AgNPs

The phytosynthesized AgNPs obtained by TF root extract were centrifuged at 15 000 rpm for 10 min to get rid of any uncoordinated biological materials [15]. UV–Vis absorption spectrum was measured using a Multiscan GO spectrophotometer (Thermo Scientific). The pellet was re-suspended in a small amount of sterilized double distilled water and then a small amount of suspension was sprayed on a glass slide to make thin film. The thin film was kept in a hot air oven to dry and then the thin film was used for the energy-dispersive x-ray spectroscopy (EDX) analysis equipped with a scanning electron microscope (SEM- JEOL JSM 6390LV, Japan) and x-ray diffractometer (XRD). Fourier transform infrared (FTIR, Perkin Elmer, Model: Spectrum 100) spectra for TF root extracts alone and AgNPs was recorded five times per scan in the frequency region 4000–400 cm^{-1} at room temperature to identify characteristic peaks and their functional groups involved in the reduction of Ag^{+} ions by KBr pellet method. Photoluminescence (PL) spectra were recorded in Vrian (Perkin Elmer, Model: LS55) spectrofluorimeter using 90° illumination. Based on the excitation maximum (340 nm), an emission scan was carried out in the range of 500–600 nm. The morphological and topographical analysis of the materials was carried out by transmission electron microscopy (FEI Technai G2 F205-TWIN TEM) and atomic force microscopy (Multiview 2000 (NSOM/SPM). The crystallinity of the nanoparticles was characterized using an x-ray diffractometer (Rigaku, Model- Miniflex) operated at a voltage of 40 kV and a current of 30 mA with Cu Kα radiation in θ–2θ configurations. The crystallinity of the particle was calculated from the width of the XRD peaks by assuming that they were free from non-uniform strains and using the Scherrer formula, $D = 0.94\ \lambda/\beta \cos\theta$, where D is the average crystallite domain size perpendicular to the reflecting planes, λ is the x-ray wavelength, β is the full width at half maximum band, θ is the diffraction angle [16].

2.3. *In vitro* anti-oxidant activity

The total phenolic content of the fractions was determined by the Folin–Ciocalteu method with slight modification [17]. The aqueous root extract and AgNPs (0.5 ml; 1 mg ml^{-1}) were mixed with Folin–Ciocalteu reagent (2.5 ml, diluted 1:10 with distilled water) for 5 min; aqueous Na_2CO_3 (2.5 ml, 75 g l^{-1}) was then added to the mixture. The mixture was allowed to stand at 25 °C for 30 min and the phenolic content was determined by spectrophotometry at 750 nm. The standard curve was prepared with 12.5, 25, 50, 100 and 200 μg ml^{-1} solutions of gallic acid (GA) in methanol. The total phenolic content was expressed as GA equivalents (mg GA g/ dry weight).

2.4. Antibacterial well diffusion assay

The antibacterial and antifungal activity of AgNPs was determined by the agar-well diffusion method against both gram-negative, gram-positive and fungal strains [18]. The microbial cultures were grown in an appropriate media and centrifuged at 5000 rpm for 5 min. Then the pellet was washed with 1X PBS and the 100 μl of the suspended culture was spread uniformly on agar plates and the plates were incubated at 4 °C for 2 h for proper diffusion of the materials. The aqueous root extracts, AgNPs alone and in combination with standard antibiotics were loaded into the wells. The anti-microbial activity was determined by measuring the diameter (mm) of the zone of growth clearance after 24 h.

2.5. *In vitro* time killing assay

To determine the antibacterial activity of the AgNPs, the overnight grown cultures were centrifuged at 5000 rpm for 5 min, washed with 1X PBS, and the pellet was suspended in LB medium. Finally the optical density of the sample was adjusted to 0.2 at 600 nm. Bacteria grown in the presence of the medium alone (control) and AgNPs (5 μM) were incubated with $2-3 \times 10^7$ CFU (colony forming units)/ml bacteria in 50 ml LB medium in triplicates. The number of CFUs were analyzed by harvesting bacteria at different time points by plating serial dilutions on LB plates, and surviving colonies were enumerated after 24 h for all bacterial strains except *M. smegmatis*, in which the colonies were enumerated after 72 h on 7H10 plates.

2.6. Bacterial cell morphology using scanning electron microscopy

SEM was performed to examine the morphological changes of two representative strains, namely *S. aureus* and *E. coli*, after incubation with AgNPs. The control and AgNPs treated bacterial cells were fixed with 2% glutaraldehyde overnight on glass coverslips. The fixed samples were then dehydrated for 30 min in a graded series of ethanol and observed by SEM.

2.7. Changes in the membrane permeability

The membrane permeability assay was examined spectrophotometrically using the protocol described previously [19]. In this study, we have chosen representative strains from gram-positive (*S. aureus*) and negative (*E. coli*) bacteria to examine the integrity of the cell membrane. Briefly, the bacterial cells grown overnight with continuous shaking in nutrient broth at 37 °C were harvested and washed with 10 mM EDTA followed by two washes with distilled water. The final absorbance of the re-suspended bacterial cells was adjusted to 0.2 at A_{600}. AgNPs and aqueous extracts (AE) were added to the bacterial suspension after incubation for 30 min at room temperature. At regular intervals of 2 h, aliquots of the samples were taken, centrifuged and the supernatants were analyzed for the presence of UV absorbing material by taking absorbance at UV_{260} and UV_{280}.

2.8. Determination of biofilm activity using crystal violet assay

We have chosen a sterile 96-well polystyrene micro titer plate (hydrophobic) as a model system to study the bacterial adhesion as reported previously [15]. Overnight grown bacterial cultures were diluted 1:100 in fresh LB medium. Different concentrations of AgNPs were added to the 96-well micro-titer plate and incubated at 37 °C for 48 h. Thereafter the medium was removed and the wells were thoroughly washed with 1X PBS and 100 μl of 0.1% (w/v) crystal violet (CV) was added and incubated for 20 min. The CV was removed and washed thoroughly with 1X PBS. For quantification of the attached cells, the CV was solubilized in absolute ethanol and the absorbance was measured at 570 nm. Reduction of the biofilm was correlated with the cells grown in the absence of AgNPs in the medium as described previously.

2.9. Effect of AgNPs on *in vitro* DNA replication fidelity using PCR

In this work, we mechanistically investigated the effects of AgNPs on *in vitro* DNA replication of small (600 bp) and large (1500 bp) DNA fragments using polymerase chain reactions (PCR). Briefly, the full length (5493 kb) of the plasmid pET-22(b^+) containing the rotavirus NSP5 gene (600 bp) was used as a template during PCR with primers (P5F 5′-ATCTAGGATCCGATGTCTCTCAGCATTGACG-3′ and P5R 5′-ATGTACTCGAGGCCAAATCTTCAATCAATTG-3′). PCR amplifications were performed in 30 μl reaction volumes with 2.5U Taq DNA polymerase, 200 μM each dNTP, and 0. 2 μM each primer and increasing concentration of AgNPs. The PCRs began with a denaturation step at 94 °C for 5 min, and 18 and 35 cycles of amplification were performed using the following conditions: 40 s at 94 °C; 30 s at 60 °C; 1 min at 72 °C. PCR amplification of 16 s rDNA was performed using genomic DNA isolated from *E. coli* (MTCC 40) with primer pairs (16 F 5′-ACATAGGATCCAGCGAACGCTGGCGGCAG-3′ and 16 R 5′-ATCTGAAGCTTTTAGCAGGTTCCCCTACGGCTA-3′). The 16S rDNA PCR consisted of an initial denaturation at 94 °C for 5 min, followed by 18 cycles of 40 s at 94 °C, 30 s at 55 °C and 1.6 min at 72 °C, and a final extension of 10 min at 72 °C.

2.10. Evaluation of biocompatibility of AgNPs using macrophages cell line (RAW 246.7) and Cucumis sativus seed germination experiment

In this study, we used the macrophage cell line RAW 246.7 to determine the biocompatible nature of AgNPs. Briefly, RAW 264.7 in DMEM was grown in a 96-well plate at 37 °C and 5% CO_2 in the presence or absence of different concentrations of AgNPs. The cell viability was determined after 24 h incubation by treating cells with MTT solution for 4 h at 37 °C in a cell culture incubator. In metabolically active cells, MTT was reduced to an insoluble dark purple formazan by mitochondrial dehydrogenases. The formazan crystals were dissolved in a denaturing buffer (SDS, HCl and isopropanol) and the absorbance was read at 570 nm in an ELISA reader. The total number of viable cells relative to the viable cells in the untreated control was calculated [17].

The germination experiment was conducted using *C. sativus* seeds surface sterilized with 10% sodium hypochlorite and then soaked in double distilled water and AgNPs suspensions separately for 2 h. To examine which process (seed soaking or incubation after the soaking) primarily retarded the various developmental stages of the seedlings, the following four treatments were given in respective petri dishes (90 mm) containing one piece of sterile filter paper with 5 ml each of AgNPs, sterile water (positive control) and TF extract alone (negative control): (a) both seed soaking and incubation were done in double distilled water; (b) both seed soaking and incubation were done in AgNPs suspension; (c) seeds soaked in double distilled water were incubated with AgNPs suspension; (d) seeds soaked in AgNPs suspension were incubated with double distilled water. Seven seeds were placed in each plate at a distance of 1 cm or larger. The above experimental treatments were allowed to germinate for 7 days until roots emerged and the seed germination rate and radical length was measured [20].

3. Results and discussion

3.1. Synthesis and characterization of AgNPs

The development of an inexpensive, reliable and eco-friendly method will help to facilitate the increasing application of noble nanoparticles that are beneficial for mankind. The yellow color of the mixture of silver nitrate and TF root extract changed rapidly to a dark brown suspended mixture after 1 h of incubation at room temperature. The formation of AgNPs was observed by the appearance of a silver surface plasmon resonance (SPR) peak at 420 nm in UV–Vis spectroscopy (figure 1(a)).

This typical SPR peak is similar to the plasmon vibrations of the AgNPs prepared by chemical reductions [21]. Similar observations of rapid biosynthesis of stable silver, gold and bi-metallic Ag/Au core–shell nanoparticles with 20 g of *Azadirachta indica* extract has been reported earlier [14]. The EDX spectrum of synthesized AgNPs clearly indicated the reduction of silver nitrate to AgNPs (figure 1(b)). The average crystalline size of AgNPs was found to be 12.95 nm and the XRD pattern demonstrated four peaks indexed to the (111) and (200), (220), and (311) Bragg reflections, which may be indicative of the face-centered cubic structure of AgNPs [15], and the AgNPs formed were essentially pure and crystalline in nature (figure 1(c)). The putative bio-molecules responsible for the green synthesis of AgNPs were identified by FTIR (figure 1(d)). The aqueous root extract of TF (black line) showed distinct peaks at 3393, 2937, 1644, 1412, 1027, and 602 cm^{-1}. Similarly, in the IR spectrum of AgNPs (red line), the peaks were observed at 3435, 2929, 1634, 1384, 1061, and 616 cm^{-1}. Comparing the IR spectra of the root extract and AgNPs, the relative shift in the distribution of peak was observed at 3393, 2937, 1644, and 1027 cm^{-1}, corresponding to carbonyl stretch (C=O, 1634 cm^{-1}), carboxylic acids (O-H, 2937 cm^{-1}) and polyphenols (O-H, 3435 cm^{-1}) functional group. The aqueous root extract of TF showed a good antioxidant activity (62.7%, figure S1(a)) as compared to the positive control- L-ascorbic acid (86.6%) using the modified DPPH scavenging assay [22]. However, the phenolic content of biosynthesized AgNPs and the extract alone as measured by the Folin–Ciocalteu method (figure S1(b), see inset) demonstrated the attachment of lower amounts (29.8 ± 1.0 mg GA g^{-1}) of phenolic compounds in AgNPs as compared to the TF root extract alone (59.6 ± 0.5 mg GA g^{-1}). The proposed mechanism for the reduction and stabilization of AgNPs might be due to the presence of polyphenols, flavonoids and other active compounds present in the root extract of TF, as schematically represented in figure 1(e). The presence of flavanoids, polyphenolic and terpenoids might be responsible for the reduction and capping of silver ions and the results correlate with the total phenolic content and IR spectral analysis (figures 1(d) and S1(b)). Polyphenolic compounds are known to possess metal chelating and reducing properties leading to the formation of metallic nanoparticles [23, 24]. AgNPs are reported to exhibit visible PL, which is shown in figure 1(e). The AgNP showed the presence of a visible PL band centered at 440 nm when excited at 300 nm wavelength and the luminescence coud be due to the presence of antioxidants present in the plant extract. The nanoparticles synthesized using olive leaf extract are also reported to be luminescent with an emission band at 425 nm and the observed PL property of AgNPs might have the potential for use in photoelectronic devices [25]. AFM and TEM micrographs revealed the diameter of AgNPs in the range of 15–30 nm (figures 2(a)–(d)). The biosynthesized nanoparticles were monodispersed,

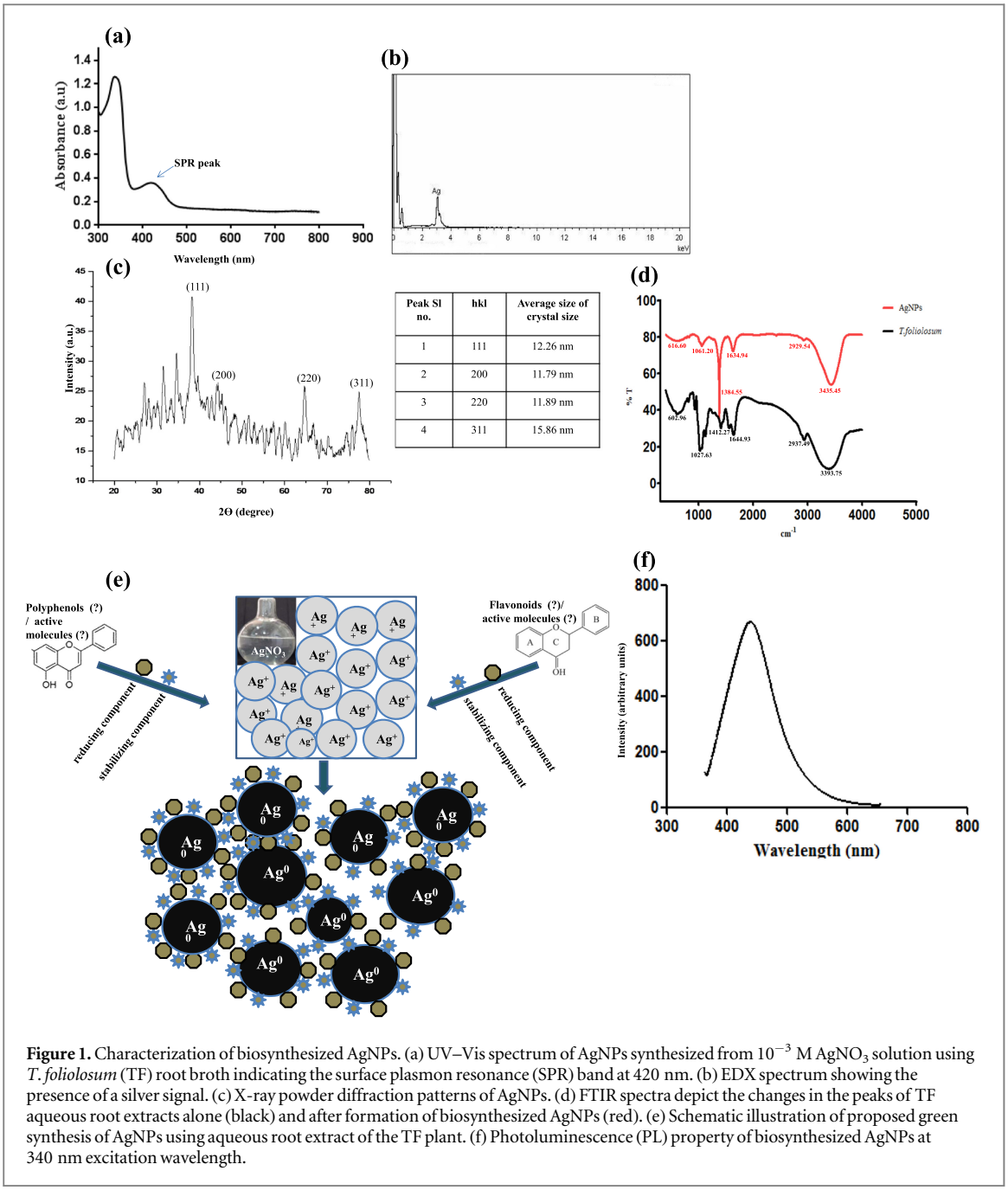

Figure 1. Characterization of biosynthesized AgNPs. (a) UV–Vis spectrum of AgNPs synthesized from 10^{-3} M $AgNO_3$ solution using *T. foliolosum* (TF) root broth indicating the surface plasmon resonance (SPR) band at 420 nm. (b) EDX spectrum showing the presence of a silver signal. (c) X-ray powder diffraction patterns of AgNPs. (d) FTIR spectra depict the changes in the peaks of TF aqueous root extracts alone (black) and after formation of biosynthesized AgNPs (red). (e) Schematic illustration of proposed green synthesis of AgNPs using aqueous root extract of the TF plant. (f) Photoluminescence (PL) property of biosynthesized AgNPs at 340 nm excitation wavelength.

roughly spherical and the agglomeration of a few AgNPs were visible as observed through AFM (figure 2(e)). The AFM micrograph shows that the particle size is bigger than those of the TEM measurements. This discrepancy could be due to the tendency of AgNPs to form an aggregate on the surface during deposition for analysis by AFM. Also, the shape of the AFM probe tip may cause misleading cross sectional views of the sample [26]. Similar to our present findings, a rapid synthesis of spherical shaped AgNPs with a dimension of 50–100 nm have been reported using the leaf extracts of *Azadirachta indica*, *Acalypha indica*, *A. dentate* and *A. indicum* [8, 9, 13, 14].

3.2. Anti-bacterial and anti-fungal activity of AgNPs

The antibacterial and antifungal effects of biosynthesized AgNPs was investigated using an agar well diffusion assay. Prior to the antimicrobial studies, the AgNPs were thoroughly washed and centrifuged to remove any unreduced Ag^+ ions. Both gram-positive bacteria (*B. subtilis* and *S. aureus*) and gram-negative bacteria (*E. coli*, *K. pneumoniae* and *P. diminuta*) showed a maximum zone of growth inhibition (table 1). Interestingly, the activity of synthesized AgNPs against clinically isolated pathogenic fungi, *T. rubrum, A. versicolor* and *C. albicans* exhibited remarkable antifungal activity with a growth inhibition diameter measuring 15–30 nm (table 1).

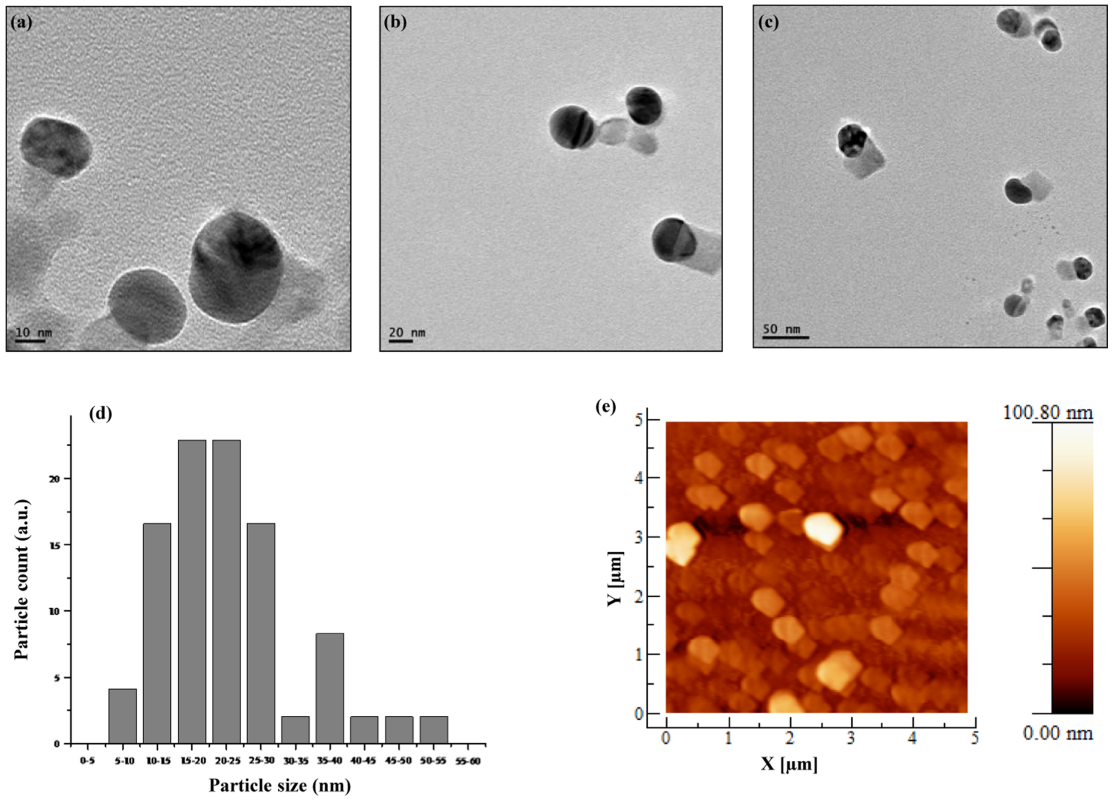

Figure 2. (a)–(d) Representative TEM micrographs of photosynthesized AgNPs. Histogram for the particle size distribution with an average mean particle size of 15–30 nm as derived by counting over multiple images. (e) The average size distribution and morphology of the silver particles were further determined by atomic force microscopy.

Table 1. Comparison of anti-microbial activity of crude AE, AgNPs alone and in combination with antibiotics against human pathogenic bacteria and fungi using agar-well diffusion assay. AE: aqueous extract; AgNPs: silver nanoparticles; ± standard deviation; ND: not determined.

	Diameter of mean zone of inhibition (mm)[a]			
Pathogenic micro-organism	AE	AgNPs	Antibiotics[#]	Antibiotic + AgNPs
Escherichia coli MTCC 40	12 ± 0.50	15 ± 0.50	19 ± 0.50	21 ± 0.50
Klebsiella pneumoniae MTCC 9038	17 ± 1.00	14 ± 0.50	22 ± 0.10	20 ± 0.50
Pseudomonas diminuta MTCC	15 ± 0.50	15 ± 0.50	19 ± 0.10	16 ± 0.50
Bacillus subtilis MTCC 121	12 ± 0.50	14 ± 0.00	19 ± 0.23	19 ± 1.00
Staphylococcus aureus MTCC 3160	—	16 ± 0.50	25 ± 0.12	24 ± 0.00
Mycobacterium smegmatis	12 ± 0.50	14 ± 0.50	23 ± 0.23	25 ± 0.50
Candida albicans MTCC 183	—	20 ± 1.00	25 ± 0.10	24 ± 0.50
Trichophyton rubrum	—	17 ± 1.00	22 ± 0.50	ND
Aspergillus versicolor	—	18 ± 0.50	22 ± 0.50	ND
Aspergillus niger	—	10 ± 0.50	22 ± 0.50	ND

[a] Antibiotics ampicillin and gentamicin were used for gram-positive and gram-negative bacteria, respectively. Nystatin was used against *C. albicans*, while the clotrimazole was used for *A. versicolor* and *T. rubrum*.

The moderate antibacterial property of the aqueous root extract of TF observed in this study might be due to the presence of antioxidant molecules (see figure S1(a)) and other secondary metabolites. However, the aqueous root extract of TF mediated biosynthesized AgNPs could increase the antibacterial and antifungal activities of active biomolecules adsorbed on AgNPs (table 1). Plants constitute an important source of numerous secondary metabolites (viz. alkaloids, tannins, flavonoids, phenolic compounds, phenolic glycosides) having bacteriostatic and bactericidal effects. Most of these secondary metabolites, other than possessing antibacterial and antifungal potential, can also act as potent antioxidants [27–29]. However, the biosynthesized AgNPs exhibited a negligible synergistic activity with the combination of standard antibiotics ampicillin, gentamicin, nystatin and clotrimazole (table 1). Figures 3(a)–(f) depict the representative agar plate images showing the clear zone of the

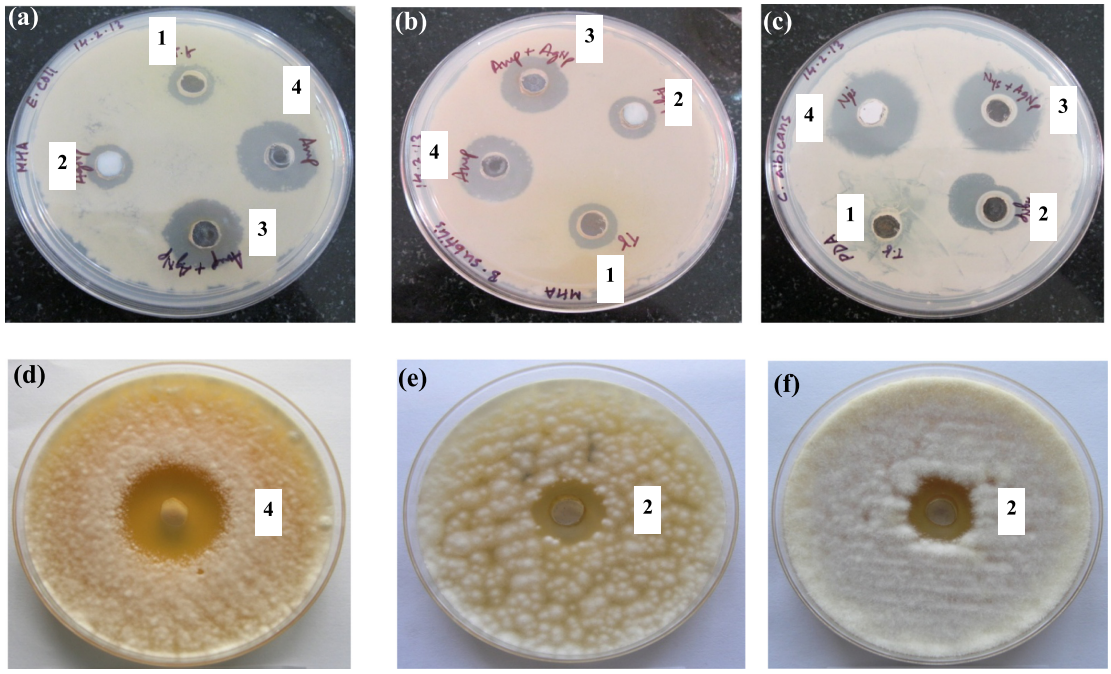

Figure 3. Photographs of semi-solid agar plates showing a clear zone of growth inhibition using crude aqueous extract (AE), AgNPs alone and in combination with antibiotics by the agar-well diffusion method. Photos of agar (bacteria) and SDA (fungi) plates inoculated with *E. coli* (a), *B. subtilis* (b), *C. albicans* (c), *A. versicolor* (d), *A. versicolor* (e), and *T. rubrum* (f), illustrating the growth inhibition zones for (1) AE alone, (2) AgNPs alone, (3) antibiotic + AgNPs, and (4) antibiotics only. Antibiotics ampicillin and clotrimazole were used as a positive control for bacteria and fungi, respectively. All the experiments were performed in triplicates.

growth inhibition of bacteria (*E. coli* and *B. subtilis*) and fungi (*C. albicans*, *A. versicolor*, and *T. rubrum*) using AE, AgNPs alone and in combination with antibiotics by the agar-well diffusion method.

The moderate synergistic effect of AgNPs with antibiotics observed in this study could be due to the lack of appropriate experimental conditions favorable for proper bonding reaction between the antibiotic and nanosilver. The antibiotic molecules contain many active groups such as hydroxyl and amido groups, which react easily with nanosilver by chelation [30]. Our results also correlate with the work previously done by some researchers where the moderate or minute increase in the inhibition zone of AgNPs against the bacteria was observed in the presence of antibiotics [31–33]. The present observation that biosynthesized AgNPs could inhibit the growth of dermatophytes correlates well with the research findings published previously [34, 35]. Intriguingly, the *M. smegmatis* cell wall is rich in lipids such as mycolic acids, which limit the binding and the permeability of drug molecules. However, the present observation of the activity of AgNPs against *M. smegmatis* corroborate with the AgNPs synthesized using gallic acid as a capping agent [36]. The bactericidal efficiency of biosynthesized AgNPs was further confirmed by performing a CFU assay against *E. coli*, *K. pneumoniae*, *P. diminuta*, *B. subtilis*, *S. aureus*, *M. smegmatis*, and *C. albicans* (figures 4(a)–(g)).

The results of the time kinetic curves revealed that AgNPs (5 μM) could significantly kill *E. coli*, *P. diminuta* and *B. subtilis* within the first 30 min of exposure to AgNPs. In contrast, the biocidal effect of AgNPs against *K. pneumoniae*, *S. aureus*, *M. smegmatis*, and *C. albicans* were observed after 2 h of incubation with AgNPs (figures 4(b), (e), (f) and (g)). The potent bactericidal activity of AgNPs may be attributed to the strong interactions between AgNPs and the macromolecules such as proteins and the DNA of bacteria [8, 9, 37, 38].

3.3. Induction of membrane damage and morphological changes in cells treated with AgNPs

SEM microscopy of two representative bacterial strains (*E. coli* MTCC 40 and *S. aureus* MTCC 3160) were carried out to observe changes in the surface morphologies of the bacterial cells after treatments with sub-inhibitory concentration of the AgNPs (5 μM) for 4 h. Native *E. coli* and *S. aureus* cells showed normal morphologies without any treatment (figures 5(a) and (b)).

Upon treatment with AgNPs, the bacterial cells underwent considerable morphological alterations as compared to the control. The results of the SEM micrographs indicated extensive damage to the cell wall, which could result in leakage of the UV absorbing material, mainly nucleic acid and protein. It can be seen that AgNPs treatment promotes the release of extracellular UV-absorbing materials, such as DNA and protein, over a period of 8 h (figures 5(c) and (d)). The results implied that the AgNPs induced the loss of UV absorbing materials from *E. coli* and *S. aureus*, probably through alteration of the membrane structure [19]. The CV assay revealed the

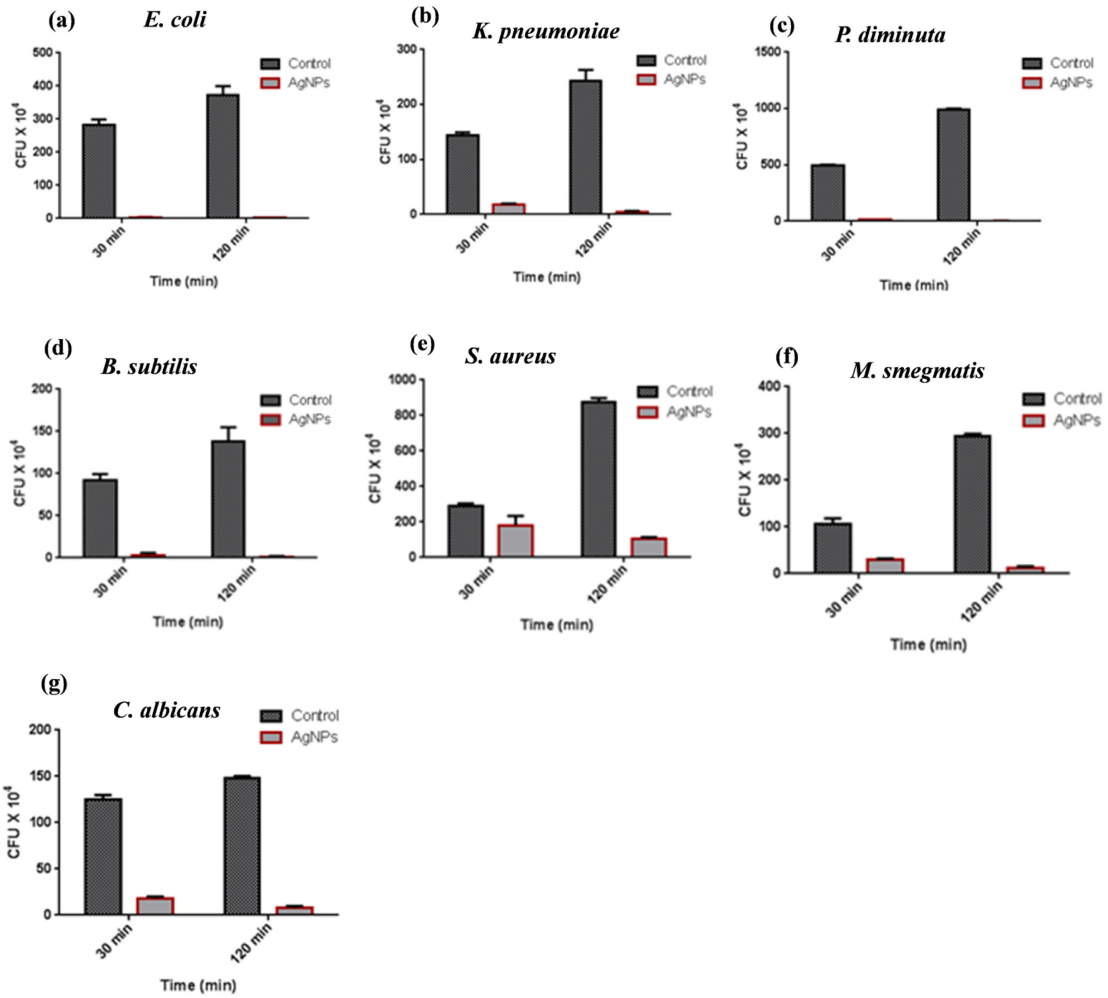

Figure 4. Time-dependent effect of AgNPs on the microbial survival using CFU assay. *E. coli* (a), *K. pneumoniae* (b), *P. diminuta* (c), *B. subtilis* (d), *S. aureus* (e), *M. smegmatis* (f) and *C. albicans* (g) were incubated in the presence of AgNPs. Microbial survival was determined at 30 min and 120 min by CFU assay. The medium containing bacteria alone was used as a control. Experiments were performed in triplicates; mean ± SD are shown.

dose-dependent (AgNPs, 312 μM and 625 μM) inhibition of biofilm formation on 96-well micro titer plates by *B. subtilis* and *S. aureus* under a given experimental set up (figures 6(a) and (b)).

A negative control with 1% DMSO did not inhibit the capacity of the bacteria to form biofilm on a polystyrene plate. The antimicrobial properties of AgNPs depend on the size and type of the capping agent used [6]. The exact mechanisms of antimicrobial properties of AgNPs are well debated and the investigations are still ongoing to understand the antibactericidal action. The positive charge on the Ag ions is suggested for antimicrobial activities of AgNPs. The high bactericidal activity might be attributed to the silver cations released from the AgNPs that probably interact with the cell wall of the bacteria, leading to increased membrane permeability [12, 37, 38]. The findings of a recent study revealed that AgNPs can simultaneously induce apoptosis in *E. coli* and inhibit new DNA synthesis in the cells in a positive concentration-dependent manner [39]. Other mechanisms involving the interaction of silver molecules with biological macromolecules, such as enzymes and DNA through an electron-release mechanism or free radical production, have been proposed [40, 41].

3.4. Role of AgNPs in suppression of DNA replication fidelity using PCR

Nanosilver is increasingly used in the food industry and biomedical applications. Several studies have implicated the potential toxicity of nanosilver through the modulation of phosphorous and sulphur containing macromolecules [40–42]. However, there is limited information on whether or how AgNPs cause changes in genetic materials. In this study, the replication fidelity of small (600 bp) and large (1500 bp) DNA fragments was quantified when nanosilver particles were present in PCRs. The results showed that the replication fidelity of a small gene was compromised by a nanosilver particle in a dose-dependent manner (figure 7(a), AgNPs (μM) concentrations used, lane 3 and 12: 53.33; lane 4 and 13: 66.67; lane 5 and 14:133.33; lane 6 and 15: 266.67; lane 7

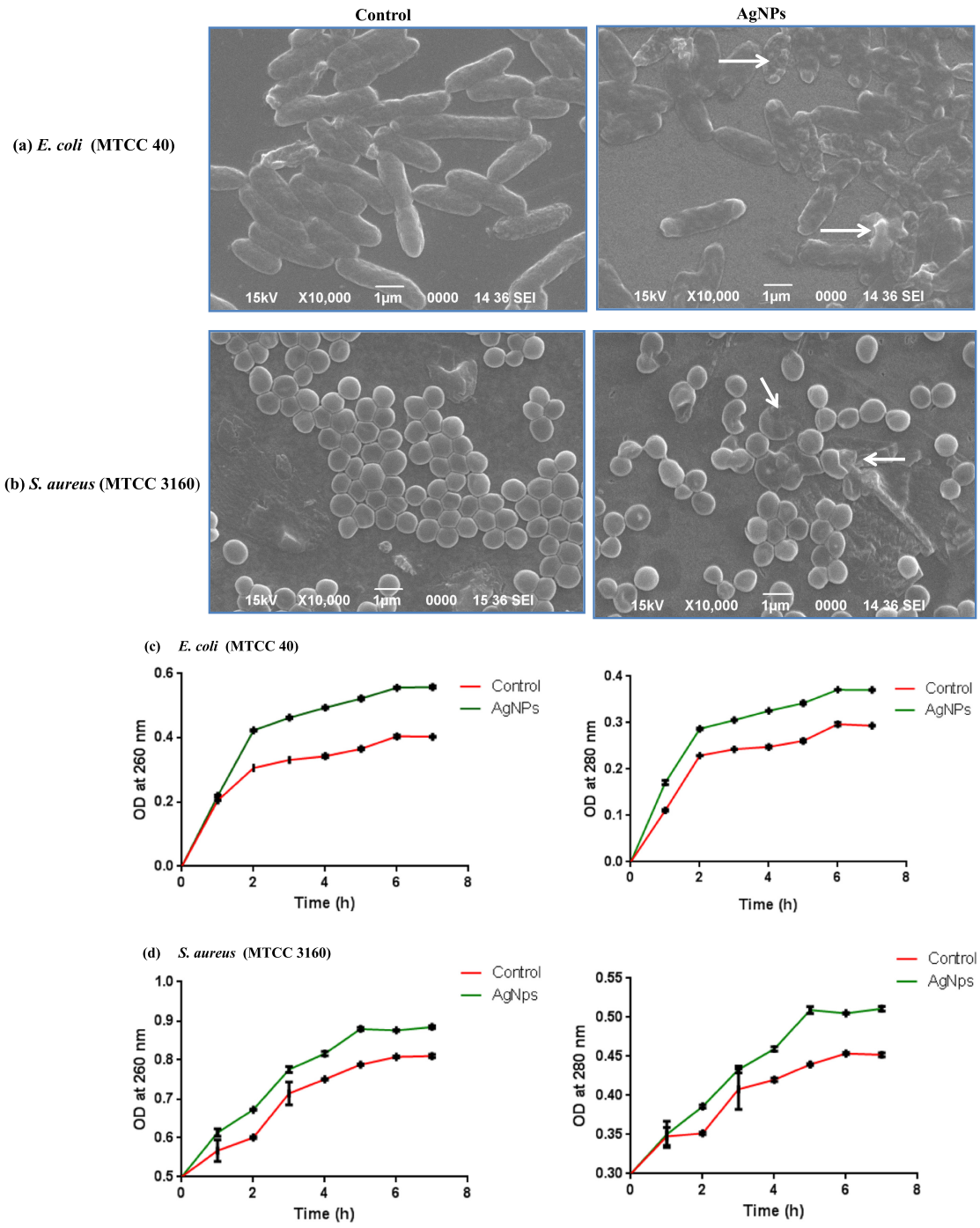

Figure 5. Morphological changes induced by AgNPs. SEM micrographs of cell structure of native *E. coli* (a) and *S. aureus* (b) cells treated with AgNPs, respectively. A solid arrow indicates morphological deformation in the treated bacterial cells. Extracellular UV-absorbing materials in *E. coli* (c) and *S. aureus* (d). Samples were taken at regular intervals following the addition of AgNPs and control cells. Data are averaged from triplicate experiments. Error bars represent standard deviations of triplicate incubations.

and 16: 400; lane 8 and 17: 533 and lane 9 and 18: 666.67) as compared to the control reaction without AgNPs at 18 and 35 cycles of PCR.

As shown in figures 7(b) and (c), adding bovine serum albumin (BSA) to PCR reactions reversed the effect of AgNPs, whereas BSA and TF extract alone had no effect on PCR (figures S2 and 7(b); lane 2: no BSA; lane 3: 2 μg ml^{-1}; lane 4: 4 μg ml^{-1}; lane 5: 8 μg ml^{-1}). This observation corrolates with the hypothesis that surface interactions between metallic nanoparticles and Taq DNA polymerase play an essential role and that BSA displaces Taq DNA polymerase from the silver surface. Gold nanoparticles were recently reported to reduce the formation of nonspecific products in PCR by hypothesized mechanisms, including adsorption of DNA and heat-transfer enhancement [43]. It was also reported that gold nanoparticles suppress the amplification of longer products while favoring amplification of shorter products, independent of specificity [44]. In contrast, we

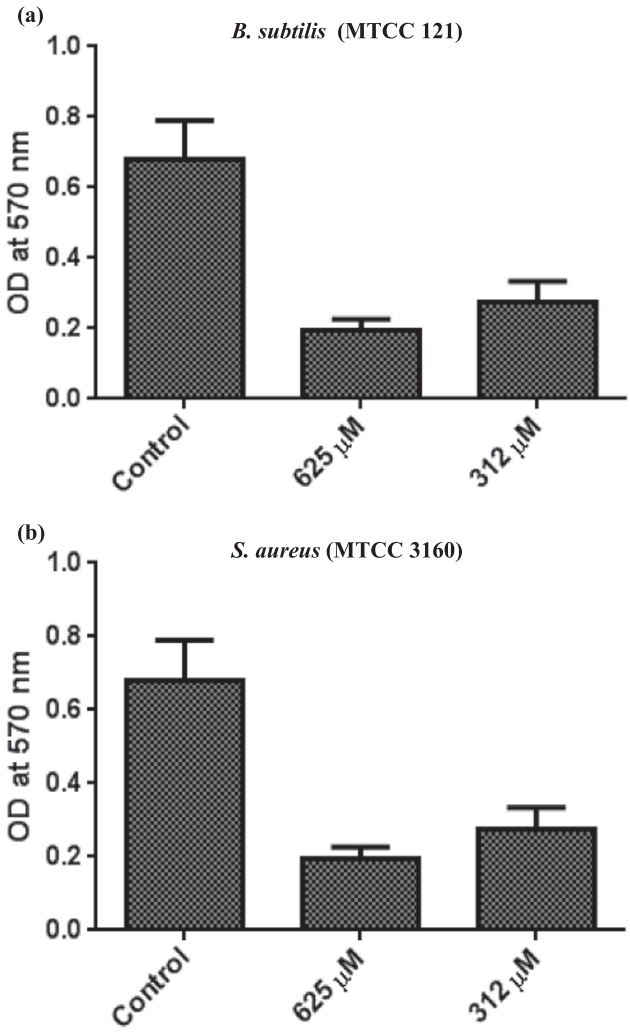

Figure 6. Ability of AgNPs on biofilm formation inhibition. Inhibition of bio-film formation by *B. subtilis* (a) and *S. aureus* (b) on 96 well plate using crystal violet assay (CV).

observed that AgNPs do suppress the amplification of both shorter and longer products in an 18 cycles PCR experiment (see figure 7(c), AgNPs concentrations (μM), lane 4: 533; lane 5 was 666.67). In concordance with observations from other research work, our experimental results imply that the nanoparticles nonspecifically adsorb polymerase, thus effectively reducing DNA polymerase concentration, leading to the suppression of amplicon size [42].

3.5. Biocompatibility of synthesized AgNPs

Despite their potent antimicrobial activity and wide biological applications, the use of AgNPs as a therapeutic agent is limited due to their potential toxic effect against mammalian cells. In this study, we tested the cytotoxicity of a plant extract that stabilized AgNPs against a macrophage cell line by the MTT assay, which relies on the fact that metabolically active cells reduce MTT to purple formazan. Untreated cells as well as cells exposed to different concentrations of the AgNPs for 24 h were subjected to the MTT assay for cell viability determination. Hence, the intensity of the dye read at 570 nm was directly proportional to the number of viable cells. AgNPs exerted no significant cytotoxic effect on mouse macrophage cell line RAW264.7 at the bactericidal concentration (5 μM), indicating that the phytochemicals present in the aqueous TF root extract provide a non-toxic capping on the AgNPs (figure 8). However, treatment with AgNPs at higher doses (10, 312, and 625 μM) resulted in approximately 10%–40% reduction in cell viability.

It is reported in the literature that different researchers showed cytotoxic effects of metallic nanoparticle preparation on mammalian cells. Gold nanoparticles showed no significant toxicity in HeLa cells [45, 46], whereas significant size-dependent toxicity was observed in fibroblasts and melanoma cells [47]. Further, it was shown that AgNPs that did not contain any capping or stabilizers exhibited a significant toxic effect on mouse macrophage J774.A1 [48], whereas starch-stabilized AgNPs had no effect on cancer cell lines U251 and

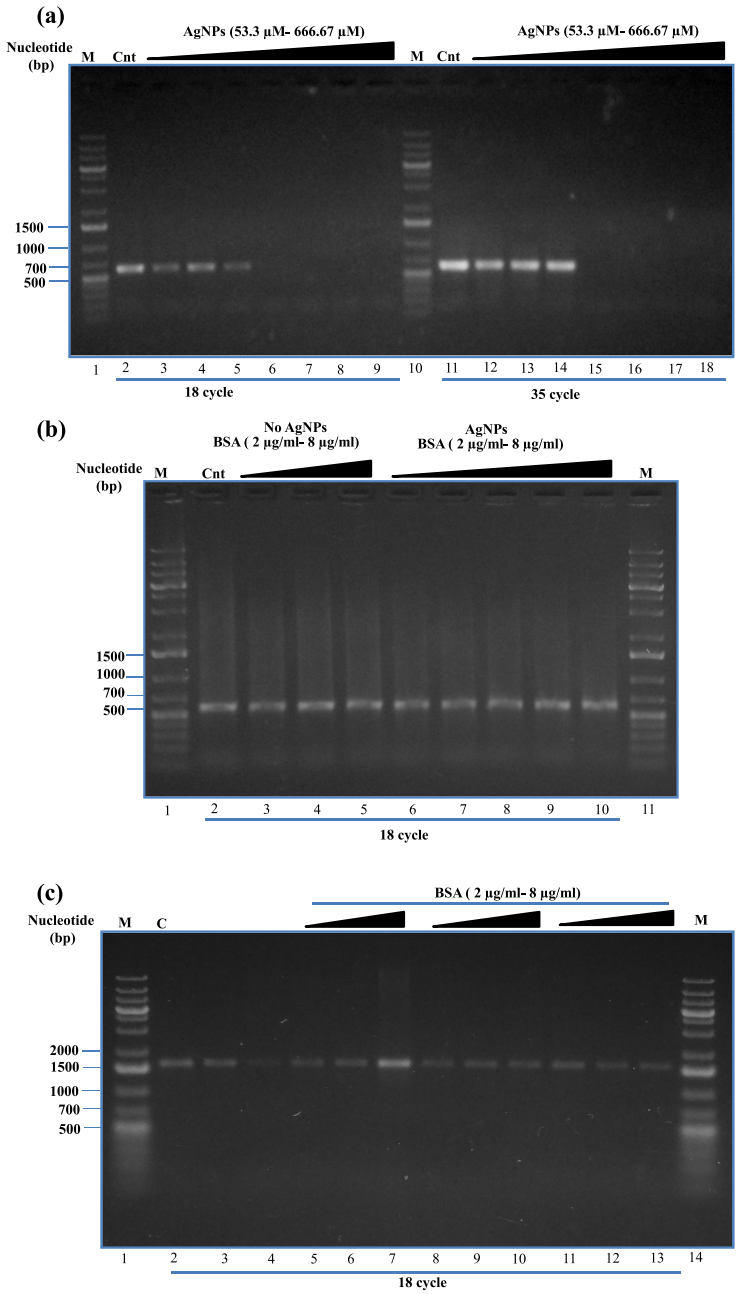

Figure 7. Effect of AgNPs on PCR amplicon length and efficiency. (a) Effect of AgNPs on PCR efficiency of small amplicon size (~600 bp). The effect of AgNPs on small size amplicon using cDNA of rotavirus gene segment 11 (Rotavirus NSP5, ~600 bp) as a template was included in the PCR experiments. Lane 1: 10 kb plus DNA ladder (Thermo Scientific); lane 2: control without AgNPs; lane 3 (increasing concentrations of AgNPs, μM): 53.33; lane 4: 66.67; lane 5:133.33; lane 6: 266.67; lane 7: 400; lane 8: 533; lane 9: 666.67 (PCR was set for 18 cycles for lanes 2 through 9); lane 10: 10 kb plus DNA ladder; lane 11: control without AgNPs; lane 12: 53.33; lane 13: 66.67; lane 14: 133.33; lane 15: 266.67; lane 16: 400; lane 17: 533; lane 18: 666.67 (PCR was set for 35 cycles for lanes 11 through 18). (b) Bovine serum albumin (BSA) reverses the effect of AgNPs on PCR efficiency irrespective of amplicon size. Lane 1: DNA ladder; lane 2: control without AgNPs and BSA; lane 3 (increasing concentrations of BSA): 2 μg ml^{-1}; lane 4: 4 μg ml^{-1}; lane 5: 8 μg ml^{-1}, lane 6: 533 μM AgNPs + 4 μg ml^{-1} BSA; lane 7: 533 μM AgNPs + 8 μg ml^{-1} BSA; lane 8: 666.67 μM AgNPs + 2 μg ml^{-1} BSA; lane 9: 666.67 μM AgNPs + 4 μg ml^{-1} BSA, and lane 10: 666.67 μM AgNPs + 8 μg ml^{-1} BSA. (c) Effect of AgNPs on PCR efficiency of large amplicon size (~1500 bp). PCRs were performed with a forward and reverse primer for 16 s rDNA (~1500 bp) using genomic DNA of *B. subtilis* as template. Lane 1: DNA ladder; lane 2: control without AgNPs and BSA; lane 3: 533 μM AgNPs; lane 4: 666.67 μM AgNPs; lane 5: 666.67 μM AgNPs + 2 μg ml^{-1} BSA; lane 6: 666.67 μM AgNPs + 4 μg ml^{-1} BSA; lane 7: 666.67 μM AgNPs + 8 μg ml^{-1} BSA; lane 8: 533 μM AgNPs + 2 μg ml^{-1} BSA; lane 9: 533 μM AgNPs + 4 μg ml^{-1} BSA, lane 10: 533 μM AgNPs + 8 μg ml^{-1} BSA; lane 11: 666.67 μM AgNPs + 2 μg ml^{-1} BSA; lane 12: 666.67 μM AgNPs + 4 μg ml^{-1} BSA and lane 13: 666.67 μM AgNPs + 8 μg ml^{-1} BSA.

fibroblasts IMR-90 [49]. In our study, seeds showing an emergence of radicle or cotyledon were recorded as being germinated to assess the phytotoxicity of AgNPs (table S1). As can be seen from table S1, the germination rate of seeds treated with AgNPs were not much affected (71.4%) as compared to the double distilled water treated seed controls (85.7%). At the gross phenotype level, AgNPs treated seedlings had shorter roots than the

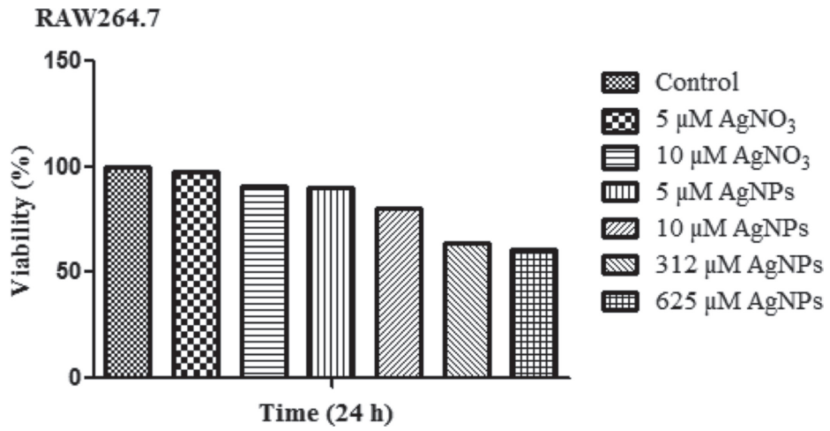

Figure 8. Cytotoxicity activity of AgNPs on mouse macrophage RAW264.7. Macrophages were treated with different concentrations of AgNPs for 24 h. Macrophages treated with and without $AgNO_3$ were used as controls. Cell viability was determined by MTT assay. Experiments were performed in triplicates; mean ± SD are shown.

controls. The observation of the present study on phytotoxicity requires further research work to understand the interaction between metal-based nanoparticles and seed coats thereby modulating the phyto-physiology.

4. Conclusions

The AgNPs synthesized using the aqueous root extract of TF is an efficient and environmentally-friendly process. AFM and TEM micrographs showed that the synthesized AgNPs were of a monodispersed spherical shape with a size range of 15–30 nm. The synthesized AgNPs revealed potent biocidal activity against bacteria and dermatophytes used in this study. The biocompatible AgNPs could be used as an antimicrobial agent in the field of biomedicine.

Acknowledgments

This research work was partially funded by the Defence Research and Development Organization, Defence Research Laboratory, Tezpur (Grant No. DRLT-P1-2012/Task-56). NDN sincerely acknowledges the Vice-Chancellor, Tezpur University for grant support through 'seed money' (TU/Fin/12-13/P/247). The biophysical characterizations of nanoparticles were performed at the Sophisticated Analytical Instrumentation Center (SAIC), Tezpur University.

Competing interests

The authors declare that they have no competing interests.

Author's contribution

SNH and KG performed the biosynthesis and antibacterial experiments. KNAMS and PB performed the effect of AgNPs on DNA replication fidelity using PCR. KKY and AN conducted the anti-fungal experiments. VV helped in analyzing the toxicity of AgNPs in cell culture. RB performed the SEM and TEM experiments. AFM characterization of the AgNPs was done in the laboratory of PD. NDN and MM designed and supervised the experiments. Some of the experiments were carried out in the laboratory of RD. NDN analyzed the whole data and wrote the manuscript.

References

[1] Popescu M, Velea A and Lorinczi A 2010 Biogenic production of nanoparticles *Dig. J. Nanomater. Bios.* **5** 1035–40
[2] Baruwati B, Polshettiwar V and Varma R S 2009 Glutathione promoted expeditious green synthesis of silver nanoparticles in water using microwaves *Green Chem.* **11** 926–30
[3] Yu D-G 2007 Formation of colloidal silver nanoparticles stabilized by Na+poly (gamma-glutamic acid)-silver nitrate complex via chemical reduction process *Colloids Surf.* B **59** 171–8

[4] Basavaraja S, Balaji D F, Lagashetty A, Rajasab A H and Venkataraman A 2008 Extracellular biosynthesis of silver nanoparticles using the fungus *Fusarium semitectum Mater. Res. Bull.* **43** 1164–70

[5] He S, Guo Z, Zhang Y, Zhang S, Wang J and Gu N 2007 Biosynthesis of gold nanoparticles using the bacteria *Rhodopseudomonas* capsulate *Mater. Lett.* **61** 3984–7

[6] Ahmed S, Ahmad M, Swami B L and Ikram S 2016 Plants extract mediated synthesis of silver nanoparticles for antimicrobial applications: a green expertise *J. Adv. Res.* **7** 17–28

[7] Mittal J, Batra A, Singh A and Sharma M M 2014 Phytofabrication of nanoparticles through plant as nanofactories *Adv. Nat. Sci: Nanosci. Nanotech.* **5** 043002

[8] Kumar D A, Palanichamy V and Roopan S M 2014 Green synthesis of silver nanoparticles using *Alternanthera dentata* leaf extract at room temperature and their antimicrobial activity *Spectrochim. Acta A* **127** 168–71

[9] Ashok Kumar S, Ravi S, Kathiravan V and Velmurugan S 2015 Synthesis of silver nanoparticles using *A. indicum* leaf extract and their antibacterial activity *Spectrochim. Acta A* **134** 34–9

[10] Panacek A, Kvıtek L, Prucek R, Kolar M, Vecerova R, Pizurova N, Sharma V K, Nevecna T and Zboril R 2006 Silver colloid nanoparticles: synthesis, characterization, and their antibacterial activity *J. Phys. Chem.* B **110** 16248

[11] Bar H, Bhui D K, Gobinda S P, Sarkar P M, Pyne S and Misra A 2009 Green synthesis of silver nanoparticles using seed extract of *Jatropha curcas Physicochem. Eng. Aspects* **348** 212–6

[12] Li W R, Xie X B, Shi Q S, Zeng H Y, Ou-Yang Y S and Chen Y B 2010 Antibacterial activity and mechanism of silver nanoparticles on *Escherichia coli Appl. Microbiol. Biotechnol.* **85** 1115–22

[13] Krishnaraj C, Jagan E G and Rajasekar S 2010 Synthesis of silver nanoparticles using *Acalypha indica* leaf extracts and its antibacterial activity against water borne pathogens *Colloids Surf.* B **76** 50–6

[14] Shankar S S, Rai A, Ahmad A and Sastry M 2004 Rapid synthesis of Au, Ag, and bimetallic Au core-Ag shell nanoparticles using Neem (*Azadirachta indica*) leaf broth *J. Colloid Interface Sci.* **275** 496–502

[15] Mohanty S, Saswati M, Prajna J, Biju J, Biplab S and Avinash S 2012 An investigation on the antibacterial, cytotoxic, and antibiofilm efficacy of starch-stabilized silver nanoparticles *Nanomed.: Nanotech. Biol. Med.* **8** 916–24

[16] Setua P, Chakraborty A, Seth D, Bhatta M U and Satyam P V 2007 Synthesis, optical properties, and surface enhanced Raman scattering of silver nanoparticles in non aqueous methanol reverse micelles *J. Phys. Chem.* C **111** 3901

[17] Ebrahimzadeh M A, Pourmorad F and Hafezi S 2008 Anti-oxidant activities of Iranian corn silk *Turk. J. Biol.* **32** 43–9

[18] National Committee for Clinical Laboratory Standards 1997 Reference method for broth dilution antifungal susceptibility testing of yeasts: Approved Standard–Third Edition, CLSI document M27-A3

[19] Heipieper H J, Diefenbach R and Kewelol H 1992 Conversion of cis unsaturated fatty acids to trans, a potential mechanism for the protection of phenol degrading *Pseudomonas putida* P8 from substrate toxicity *Appl. Environ. Microbiol.* **58** 1847–52

[20] Rocktotpal K, Niranjan K, Sawian C E, Baruah S and Mandal M 2011 Effect of sonication and aging on the templating attribute of starch for green silver nanoparticles and their interactions at bio-interface *Carbohydrate Polymers* **83** 1245–52

[21] Jiang H, Manolache S, Lee Wong C and Denis F S 2004 Plasma-enhanced deposition of silver nanoparticles onto polymer and metal surfaces for the generation of antimicrobial characteristics *J. Appl. Polymer Sci.* **93** 1411–22

[22] Paul S, Saikia J P, Samdarshi S K and Konwar B K 2009 Investigation of antioxidant property of iron oxide particles by 1′-1′ diphenylpicryl-hydrazyle (DPPH) method *J. Magn. Magn. Mater.* **321** 3621

[23] Dipankar C and Murugan S 2012 The green synthesis, characterization and evaluation of the biological activities of silver nanoparticles synthesized from Iresine herbstii leaf aqueous extracts *Colloids Surf. B* **98** 112–9

[24] Sadeghi B and Gholamhoseinpoor F 2015 A study on the stability and green synthesis of silver nanoparticles using Ziziphora tenuior (Zt) extract at room temperature *Spectrochim. Acta A* **134** 310–5

[25] Khalil M M H, Ismail E H and El-Magdoub F 2012 Biosynthesis of Au nanoparticles using olive leaf extract. first nano updates *Arab. J. Chem.* **5** 431e437

[26] Alahmad A, Eleoui M, Falah A and Alghoraibi I 2013 Preparation of colloidal silver nanoparticles and structural characterization *Phys. Sci. Res. Int.* **4** 89–96

[27] Venkata S P, Murali M C, Prameela K, Sravani R and Raju B A 2012 Screening of antimicrobial and antioxidant potentials of *Acacia caesia*, *Dillenia pentagyna* and *Buchanania lanzan* from Maredumilli Forest of India *J. Pharm. Res.* **5** 1734–8

[28] Ibtissem B, Abdelly C and Sfar S 2012 Antioxidant and antibacterial properties of *Mesembryanthemum crystallinum* and *Carpobrotus edulis* extracts *Adv. Chem. Eng. Sci.* **2** 359–65

[29] Vasconcelos M A *et al* 2014 Antibacterial and antioxidant activities of derriobtusone A isolated from *Lonchocarpus obtusus Biomed. Res. Int.* **2014** 248656

[30] Fayaz A M, Balaji K, Girilal M, Yadav R, Kalaichelvan P T and Venketesan R 2010 Biogenic synthesis of silver nanoparticles and their synergistic effect with antibiotics: a study against gram-positive and gram-negative bacteria *Nanomedicine: Nanotech. Biol. Med.* **6** 103–9

[31] Ghosh S *et al* 2012 Synthesis of silver nanoparticles using *Dioscor ea bulbifera* tuber extract and evaluation of its synergistic potential in combination with anti-microbial agents *Int. J. Nanomed.* **7** 483–96

[32] Jyoti K, Baunthiyal M and Singh A 2015 Characterization of silver nanoparticles synthesized using *Urtica dioica* Linn. leaves and their synergistic effects with antibiotics *J. Rad. Res. Appl. Sci.* **9** 217–27

[33] Kim K J, Sung W S, Moon S K, Choi J S, Kim J G and Lee D G 2008 Antifungal effect of silver nanoparticles on dermatophytes *J. Microbiol. Biotechnol.* **18** 1482–4

[34] Kim K J, Sung W S, Suh B K, Moon S K, Choi J S, Kim J G and Lee D G 2009 Antifungal activity and mode of action of silver nanoparticles on *Candida albicans Biometals* **22** 235–42

[35] Martinez-Gutierrez F, Olive P L, Banuelos A, Orrantia E, Nino N, Sanchez E M, Ruiz F, Bach H and Av-Gay Y 2010 Synthesis, characterization, and evaluation of antimicrobial and cytotoxic effect of silver and titanium nanoparticles *Nanomed.* **6** 681–8

[36] Feng Q L, Wu J, Chen G Q, Cui F Z, Kim T N and Kim J O 2000 A mechanistic study of the antibacterial effect of silver ions on *Escherichia coli* and *Staphylococcus aureus J. Biomed. Mater. Res.* **52** 662–8

[37] Li W-R, Xie X-B, Shi Q-S, Zeng H-Y, OU-Yang Y-S and Chen Y-B 2010 Antibacterial activity and mechanism of silver nanoparticles on *Escherichia coli Appl. Microbiol. Biotechnol.* **85** 1115–22

[38] Dibrov P, Dzioba J, Gosink K K and Hase C C 2002 Chemiosmotic mechanism of antimicrobial activity of Ag (+) in Vibrio cholerae *Antimicrob. Agents Chemother.* **46** 2668–70

[39] Bao H, Yu X, Xu C, Li X, Li Z, Wei D and Liu Y 2015 New toxicity mechanism of silver nanoparticles: promoting apoptosis and inhibiting proliferation *PLoS One* **10** e0122535

[40] Sharma V K, Yngard R A and Lin Y 2009 Silver nanoparticles: green synthesis and their antimicrobial activities *Adv. Colloid Interface Sci.* **145** 83–96
[41] Park J, Lim D H, Lim H J, Kwon T, Choi J S, Jeong S, Choi I H and Cheon J 2011 Size dependent macrophage responses and toxicological effects of Ag nanoparticles *Chem. Commun.* **47** 4382–4
[42] Yang W, Shen C, Ji Q, An H, Wang J, Liu Q and Zhang Z 2009 Food storage material silver nanoparticles interfere with DNA replication fidelity and bind with DNA *Nanotech.* **20** 085102
[43] Li M, Lin Y C, Wu C C and Liu H S 2005 Enhancing the efficiency of a PCR using gold nanoparticles *Nucleic Acids Res.* **33** e184
[44] Vu B V, Litvinov D and Willson R C 2008 Gold nanoparticle effects in polymerase chain reaction: favoring of smaller products by polymerase adsorption *Anal. Chem.* **80** 5462–7
[45] Hauck T S, Ghazani A A and Chan W C 2008 Assessing the effect of surface chemistry on gold nanorod uptake, toxicity, and gene expression in mammalian cells *Small* **4** 153–9
[46] Jameel A K, Beena P, Das T K, Singh Y and Maiti S 2007 Molecular effects of uptake of gold nanoparticles in HeLa Cells *Chem. Bio. Chem.* **8** 1237–40
[47] Pan Y, Neuss S, Leifert A, Fischler M, Wen F, Simon U, Schmid G, Brandau W and Jahnen-Dechent W 2007 Size-dependent cytotoxicity of gold nanoparticles *Small* **3** 1941–9
[48] Yen H J, Hsu S H and Tsai C L 2009 Cytotoxicity and immunological response of gold and silver nanoparticles of different sizes *Small* **5** 1553–61
[49] Asha Rani P V, Low Kah Mun G, Hande M P and Valiyaveettil S 2009 Cytotoxicity and genotoxicity of silver nanoparticles in human cells *ACS Nano* **24** 279–90